Electronic Supplementary Material (ESI) for Materials Horizons.
This journal is © The Royal Society of Chemistry 2024

Supporting Information

Transition Metal-substituted Polyoxometalate-Ionic Liquids as High-Performance Flame Retardants for Epoxy Resins

Ying Zeng,[a] Yeqin Feng,[a] Junhao Zhang,[a] Carsten Streb,[b]* Zhimin Wang,[a] Hongjin Lv,[a]* and Guo-Yu Yang[a]

[a] Dr. Y. Zeng, Y. Feng, J. Zhang, Z. Wang, Prof. H. Lv,* Prof. G.-Y. Yang

MOE Key Laboratory of Cluster Science, Beijing Key Laboratory of Photoelectric/Electrophotonic Conversion Materials, School of Chemistry and Chemical Engineering, Beijing Institute of Technology, Beijing 102488, China

E-mail: hlv@bit.edu.cn

[b] Prof. C. Streb

Department of Chemistry, Johannes Gutenberg University Mainz, Duesbergweg 10-14, 55128 Mainz, Germany

E-mail: carsten.streb@uni-mainz.de

Table of contents

1. Materials

All chemicals for synthesis of transition-metal-substituted polyoxometalates (tmsPOMs) and transition-metal-substituted polyoxometalate ionic liquids (tmsPOM-ILs) were purchased from Alfa Aesar, Meryer, or Macklin and used without further purification unless stated otherwise. The tungstophosphate precursor salt, [*B*-PW_9O_{34}]$^{9-}$, was prepared according to the literature.[1] Bisphenol A diglycidyl ether (D.E.R.™ 332, BADGE) and 4,4'-Diaminodiphenylmethane (DDM, > 97.0 %), purchased from Sigma Aldrich, were used for preparation of epoxy resin as received.

2. Synthesis and characterization

2.1. Synthesis of $K_6P_2W_{18}O_{62}$ (K^+-P_2W_{18}).[1] A solution of $Na_2WO_4 \cdot 2H_2O$ (20 g, 60.6 mmol) in 70 mL of water was heated to boiling, and to this boiling solution was slowly added 30 mL of 85% H_3PO_4. The resulting yellow-green solution was refluxed for 8 h and then cooled to room temperature. 20 g of solid KCl was added to the cooled solution, and the precipitation was collected and redissolved in a minimum amount of hot water to allow for crystallization at 5 °C overnight. Light green crystals were obtained by filtration and vacuum-dried at 80 °C for 2 h. Yield: 13.6 g (87.9 % based on W).

2.2. Synthesis of $K_{10}[Zn_4(H_2O)_2(B\text{-}PW_9O_{34})_2]\cdot 20H_2O$ (K^+-Zn_4).[1] Solid $ZnCl_2$ (0.19 g, 1.4 mmol) was dissolved in 15 mL of water. 2.0 g of solid [*B*-PW_9O_{34}]$^{9-}$ (0.8 mmol) were added to the solution, and the solution was heated under vigorous stirring until a homogeneous translucent white solution resulted. Any precipitate was removed by hot gravity filtration and 5 g of solid KCl were added to the clear filtrate. The precipitation of a white solid was collected at room temperature and redissolved in 10 mL of hot water to recrystallize overnight at 5 °C. White crystalline powder was collected and vacuum-dried at 80 °C for 2 h. Yield: 1.6 g (83.0 % based on Zn).

2.3. Synthesis of $Na_3K_7[Cu_4(H_2O)_2(B\text{-}PW_9O_{34})_2]\cdot 30H_2O$ (Na^+K^+-Cu_4).[2] Solid $CuCl_2\cdot 2H_2O$ (0.62 g, 3.6 mmol) was added to 12 mL of water, and to this light blue solution was added solid $[B\text{-}PW_9O_{34}]^{9-}$ (5.1 g, 1.8 mmol) with vigorous stirring until all the $[B\text{-}PW_9O_{34}]^{9-}$ was dissolved. 1 g of solid KCl was added to the clear light green solution, resulting in the precipitation of a pale green solid. The resulting precipitates were collected by centrifugation, redissolved in 30 ml of warm water, and allowed to crystallize overnight at 4 °C. Pale green needle-shaped crystals were collected by filtration and air-dried at room temperature. Yield: 1.8 g (36 % based on Cu).

2.4. Synthesis of $Na_6K_4[Ni_4(H_2O)_2(PW_9O_{34})_2]\cdot 32H_2O$ (Na^+K^+-Ni_4).[3] Solid $Na_2WO_4\cdot 2H_2O$ (33 g, 100 mmol) and solid Na_2HPO_4 (1.57 g, 11 mmol) were dissolved in 100 mL water. The pH of the solution was adjusted to 7.2 by addition of concentrated acetic acid. A solution of $Ni(OCOCH_3)_2\cdot 4H_2O$ (5.5 g, 22 mmol) in 50 mL water was then added slowly under vigorous stirring and the resultant mixture was refluxed for 2.5 h. Any precipitate was removed by hot gravity filtration and 4 g of solid $K(OCOCH_3)$ was added to the filtrate. The resulting hot yellow solution was left for crystallization at room temperature. Chartreuse crystalline powder was collected by filtration and air-dried at room temperature. Yield: 19.8 g (64 % based on Ni).

2.5. Synthesis of $((n\text{-}C_7H_{15})_4N)_{10}[M_4(H_2O)_2(B\text{-}\alpha\text{-}PW_9O_{34})_2]$ (THA-M_4, M=Cu, Ni, or Zn) and $((n\text{-}C_7H_{15})_4N)_6[P_2W_{18}O_{62}]$ (THA-P_2W_{18}). It is well-established that most POMs can be quantitatively extract from the aqueous phase to a second organic phase through cation-exchange process.[4] Typically, the desired polyoxometalate salt (Na^+K^+-Cu_4, Na^+K^+-Ni_4, or K^+-Zn_4, 5 g, 0.9 mmol, 1 eq.) was dissolved in 80 mL water. A solution of tetraheptylammonium bromide (THA-Br, 4 g, 8.0 mmol, 9 eq.) in 20 mL dichloromethane was added. The mixture was vigorously stirred for half an hour and the organic layer was then separated for further removal of the solvent using a rotary evaporator. The resulting viscous liquid was thoroughly washed twice with 50 mL water and twice with 50 mL ether. Procedures

identical to the above were followed to prepare **THA-P_2W_{18}** except that a smaller amount of THA-Br (2.7 g, 5.4 mmol, 5 eq.) was used. Yield: **THA-Cu_4**, 6.4 g (80 % based on Cu); **THA-Ni_4**, 6.7 g (84 % based on Ni); **THA-Zn_4**, 6.2 g (78 % based on Zn); **THA-P_2W_{18}**, 5.5 g (74 % based on W).

2.6. Preparation of epoxy resin (EP) and its composites (EP/FR-*x*). The composites (EP/FR-*x*, where FR represents the additive flame retardant and *x* is the mass content of the additive in the composite) were prepared by a traditional thermal curing process. Taking the preparation of **EP/THA-Cu_4-3** as an example, viscous liquid D.E.R.™ 332 (30 g) and the additive **THA-Cu_4** (1.186 g, 3 wt.%) were mixed at 90 °C with vigorous stirring until a clear transparent solution was obtained. The solution was degassed under vacuum, followed by rapidly dumping into liquid DDM (8.36 g) at 90 °C. After continuous stirring to get a homogenous solution, the mixture was degassed under vacuum and then poured into a preheated Teflon mold for curing. The curing program was set as 100 °C for 2 h, 150 °C for 2 h, and then cooled naturally to room temperature. Procedures identical to the above were followed to prepare pure epoxy resin or other composites, except that different kinds and amounts of additives were included.

2.7. Characterization. The vibrational signatures of the tmsPOMs and the tmsPOM-ILs were identified by a Fourier-transform infrared spectrometer (FTIR, Bruker Tensor II). Each measurement was from 500 to 4000 cm^{-1} with a resolution of 4 cm^{-1}. Differential scanning calorimetry (DSC) was carried out to study the curing behavior of the EP/tmsPOM-IL composites, and the samples (around 15 mg) were heated from 25 °C to 250 °C on a Mettler Toledo DSC 3 with a heating rate of 10 °C/min under a nitrogen atmosphere. Dynamic mechanical analysis (DMA) was performed with a three-point bending pattern on a TA Q800 instrument, and the samples (55 mm × 6.5 mm × 3 mm) were tested from 25 °C to 250 °C with a heating rate of 10 °C/min, a constant frequency of 1.0 Hz, and an oscillation amplitude of 10.0 μm. The fire-resistance performance of the epoxy and its composites was evaluated by a butane

torch test with a sample size of Ø40 mm × 10 mm. An infrared camera TiS75+ (Fluke, -10 to 550 °C) was used to acquire the backside temperatures of the samples. The butane torch test was stopped when the sample was penetrated by the torch flame and the backside temperature went beyond the temperature range of the camera. An oxygen index analyzer (Fire Testing Technology) was used to measure the limiting oxygen index (LOI) values of the epoxy and its composites according to ASTM D2863 with a sample size of 100 mm × 6.5 mm × 3 mm. The self-extinguishing and anti-dripping performance were evaluated by the UL-94 vertical burning test (Motis Fire Technology) according to ASTM D3801 with a sample size of 125 mm × 13 mm × 3 mm. Cone calorimetry (Fire Testing Technology) was conducted to analyze the heat and smoke release during combustion according to ISO 5660 with a sample size of 100 mm × 100 mm × 3 mm at a heat flux of 35 kW/m^2. The microstructures of samples were observed using scanning electron microscopy (SEM, Zeiss Supra 55) at an acceleration voltage of 20 kV, and the energy dispersive X-ray spectrometer (EDX) for elemental analysis was conducted on a Hitachi SU-8020 with a surface scanning model. Thermogravimetric analyses (TGA) were carried out to study the thermal degradation of the epoxy and its composites, using a Netzsch STA 449 F3 Jupiter operated from room temperature to 800 °C with a heating rate of 10 °C/min under a nitrogen atmosphere. Thermogravimetry coupled with Fourier-Transform-Infrared spectroscopy (TG-FTIR, Mettler Toledo TGA/DSC 3+) was adopted to analyze the pyrolysis products of the epoxy and its composites. The heating program was set from room temperature to 800 °C with a heating rate of 10 °C/min under a nitrogen atmosphere. Tensile properties were measured with an electronic universal testing machine (DXLL-5000, Shanghai D & G Measure Instrument Co. Ltd.) according to ASTM D638 at a crosshead speed of 2 mm/min. Raman spectroscopy (Renishaw inVia) was used to identify the graphitization of the char residues with an argon laser of 514 nm in a wavelength range from 500 to 2000 cm^{-1}. The elemental chemical states of the samples were analyzed by X-ray photoelectron spectroscopy (XPS, PHI Quantera II SXM), using an X-ray source of Al Kα radiation (1486.6 eV, line width 0.68 eV). Accelerated

aging tests were adopted to assess the migration resistance of the EP/tmsPOM-IL composites. The samples were immersed in deionized water at 60 °C to mimic a humid and hot atmosphere, and the aging times were set to 24 h, 72 h, and 168 h.

3. Analyses

3.1. Characterization of structure, morphology, and mechanical performance

Figure S1 shows the FT-IR spectra of Na^+K^+-M_4 and THA-M_4 (M=Ni, Cu). The characteristic peaks at 1043 cm^{-1} (P-O, restoration of tetrahedral symmetry after metal substitution), 945 cm^{-1} (W-O, terminal), and 900-700 cm^{-1} (W-O-W, bridging) indicate the structure of the metal-substituted sandwich-type POM cluster.[1] After the cation metathesis between Na^+K^+-M_4 and THA-Br, the peaks at 3050-2750 cm^{-1} (C-H, ν), 1464 cm^{-1} (C-H, δ), and 723 cm^{-1} (C-N, ν) appear in the spectra of THA-M_4. Figure S2 presents the full-scan XPS spectra of THA-Ni_4 and THA-Cu_4, indicating the presence of C, N, O, and W in their elemental composition. High-resolution spectra of Ni 2p and Cu 2p further confirm the being of Ni(II) and Cu(II) in THA-Ni_4 and THA-Cu_4, respectively. The FT-IR and XPS results proved the successful synthesis of the transition-metal-substituted polyoxometalate salts (tmsPOMs) and the transition-metal-substituted polyoxometalate-based ionic liquids (tmsPOM-ILs). In the preparation of the EP/tmsPOM-IL composites, the tmsPOM-IL were found to be fully miscible with the epoxy resin, leading to the retained transparency of the cured composites. The fracture surfaces of the EP and EP/tmsPOM-IL composites were characterized by the SEM images (Figure S3). Similar smooth and brittle fracture surfaces were observed in the images of the epoxy and its composites. The strong resemblance between the fracture surfaces accords with the visual transparency of the EP/tmsPOM-IL composites. Tensile tests were conducted to investigate the effects of the tmsPOM-ILs on the mechanical properties of the epoxy resin. The representative stress-strain curves and the corresponding results of the EP and EP/tmsPOM-IL composites are presented in Figure S4. Compared to the pure epoxy resin (55.2 MPa), the addition of the

tmsPOM-IL barely changed the tensile strength of the composites (54.8 MPa for **EP/THA-Ni$_4$** and 56.7 MPa for **EP/THA-Cu$_4$**). These results plainly indicate that the counter-cation of the tmsPOMs with long-chain alkyls successfully tuned the compatibility of the EP/tmsPOM-IL system and thereby conserved the intrinsic morphological characteristics and tensile properties of the epoxy resin to the greatest extent.

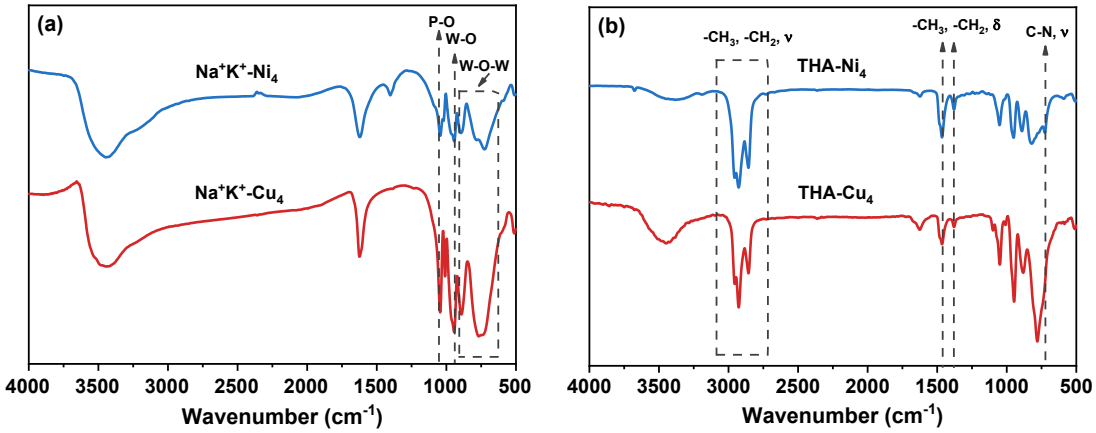

Figure S1. FT-IR spectra of (a) Na^+K^+-M_4 and (b) THA-M_4 (M=Ni, Cu).

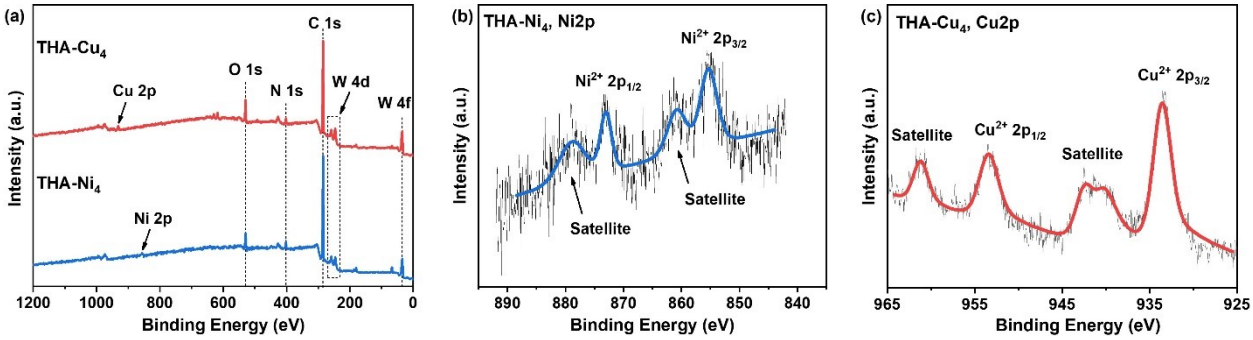

Figure S2. Full-scan XPS spectra (a) of THA-Ni$_4$ and THA-Cu$_4$ and their corresponding high-resolution XPS spectra of (b) Ni 2p and (c) Cu 2p.

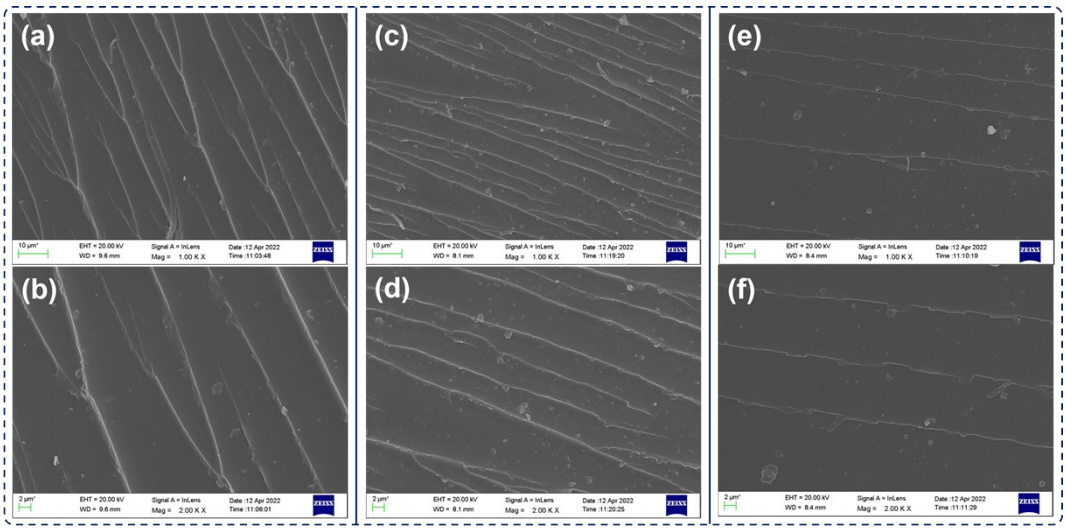

Figure S3. Fracture surfaces of **EP** (a, b), **EP/THA-Ni$_4$** (c, d), and **EP/THA-Cu$_4$** (e, f) observed with SEM.

Table S1. Detailed DMA data of EP and EP/tmsPOM-IL composites.

Sample	T_g (°C)	E' (MPa)[a]	v_e (×10^3, mol/m^3)[b]
EP	165	38.15	3.44
EP/THA-Ni$_4$-3	157	43.55	3.79
EP/THA-Cu$_4$-3	157	49.20	4.36

[a] E' denotes the storage modulus at T_g+30 °C in the rubbery plateau.

[b] v_e represents the crosslinking density, calculated with the equation: v_e=E'/3R(T_g+30), R is the ideal gas constant.

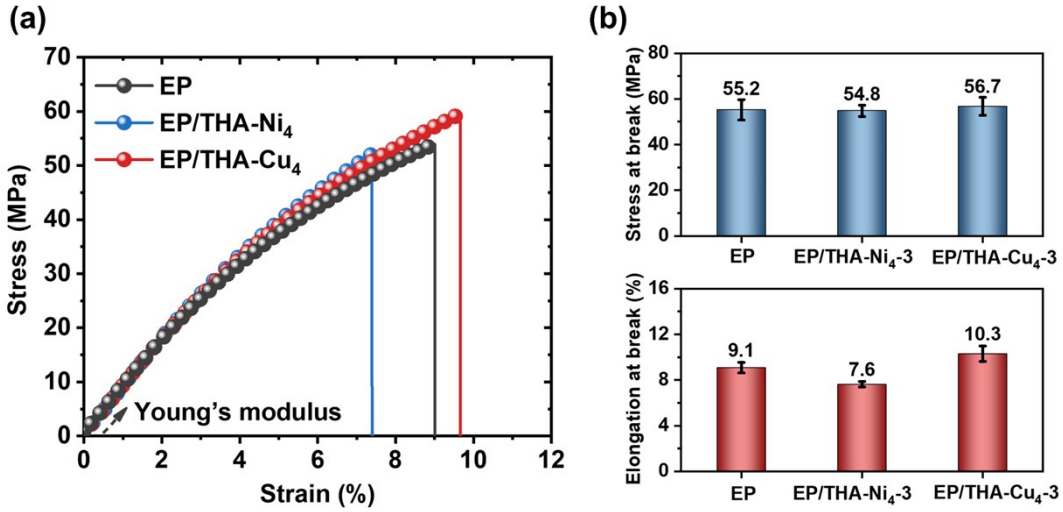

Figure S4. Representative stress-strain curves (a) and tensile properties (b) of **EP**, **EP/THA-Ni$_4$**, and **EP/THA-Cu$_4$.**

3.2. Thermal stability

The thermal stability of the **THA-Ni$_4$**, **THA-Cu$_4$**, EP, and EP/tmsPOM-IL composites was assessed by thermogravimetric analyses under air and nitrogen atmospheres (Figure S5, Figure S6, Tables S2 and S3). Both the EP/tmsPOM-IL composites, especially in the case of the **EP/THA-Cu$_4$-3**, exhibited decreased maximum decomposition rate at temperatures higher than that of the pure epoxy resin and yielded increased residual weight at 800 °C.

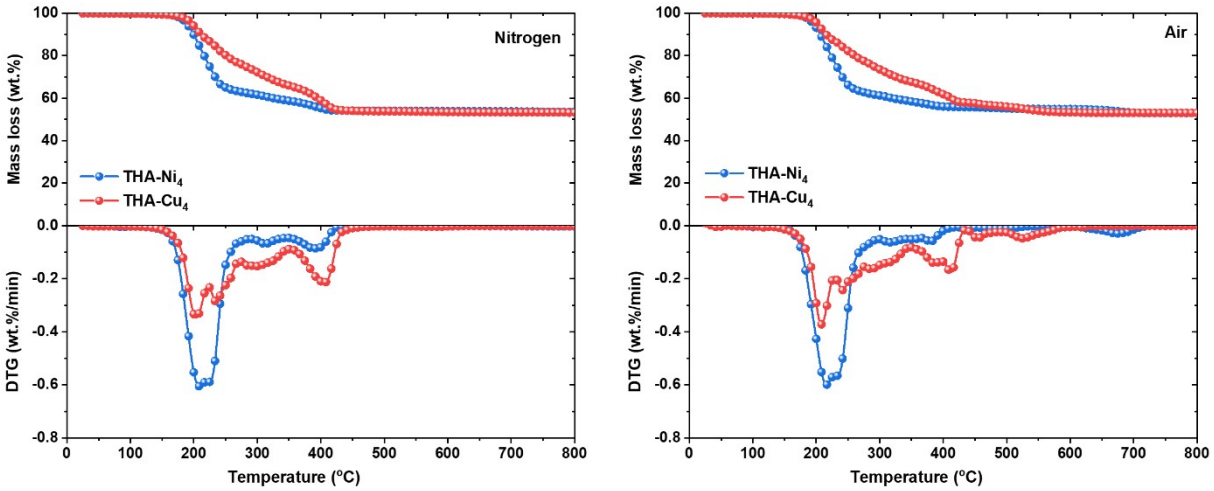

Figure S5. Mass loss and mass loss rate of **THA-Cu$_4$** and **THA-Ni$_4$** under nitrogen and air atmospheres.

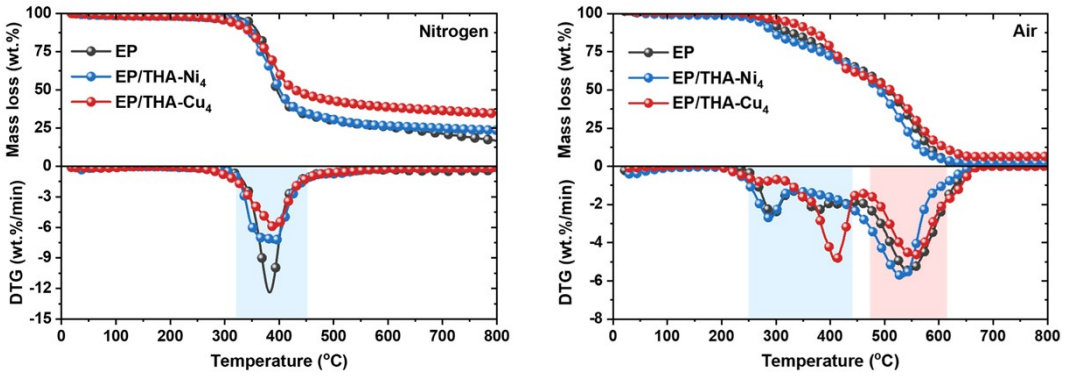

Figure S6. Mass loss and mass loss rate (DTG) curves of the epoxy resin and its composites under nitrogen and air atmospheres. The colored rectangles highlight the decomposition regions.

Table S2. Detailed TGA data of the epoxy resin and its composites under a nitrogen atmosphere.

Sample	$T_{-5\%}$[a] (°C)	T_{max}[b] (°C)	Residue at 800 °C (wt.%)
EP	341.9	382.5	16.7
EP/THA-Ni$_4$-3	324.7	389.5	23.5
EP/THA-Cu$_4$-3	306.3	392.0	34.5

[a] $T_{-5\%}$ denotes the temperature where 5 % weight loss.

[b] T_{max} represents the temperature where the maximum mass loss occurred.

Table S3. Detailed TGA data of the epoxy resin and its composites under air.

Sample	$T_{-5\%}$ (°C)	T_{max1} (°C)	T_{max2} (°C)	Residue at 800 °C (wt.%)
EP	282.2	294.5	544.7	0
EP/THA-Ni$_4$-3	255.9	288.6	533.7	2.4
EP/THA-Cu$_4$-3	290.5	409.8	553.3	6.5

3.3. Fire-safety properties

The fire-resistance performance of the epoxy resin and its composites in the butane torch test is illustrated with the photographic images and infrared satellite images at different times (Figures S7 and S8). Compared to the case of the pure epoxy resin, the composites, owing to the incorporation of the tmsPOM-ILs, presented less severe combustion and lasted longer before the torch flame penetrated the sample (2.6, 12.6, and 23.8 min for **EP**, **EP/THA-Ni$_4$-3**, and **EP/THA-Cu$_4$-3**, respectively).

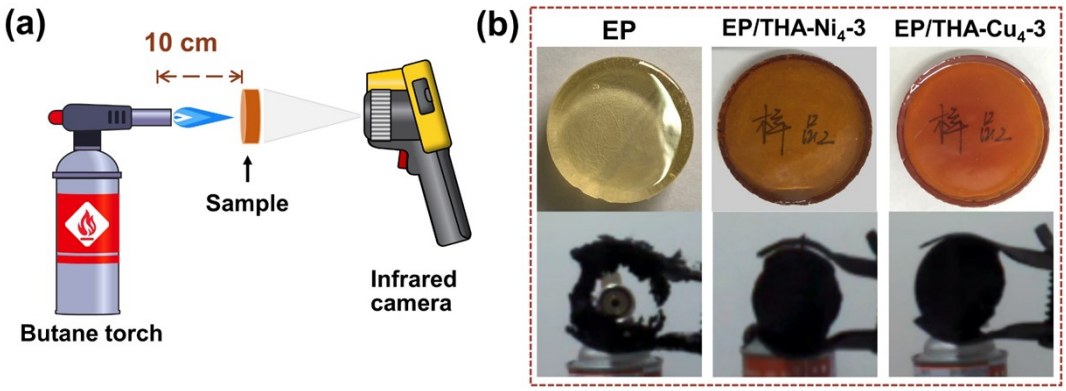

Figure S7. Fire-resistance performance of epoxy resin and its composites with exposure to a flame of a butane torch. (a) Illustration of the setup for the test and the measurement of the backside temperature of the sample. (b) Samples before (Ø40 mm × 10 mm) and after the butane torch test.

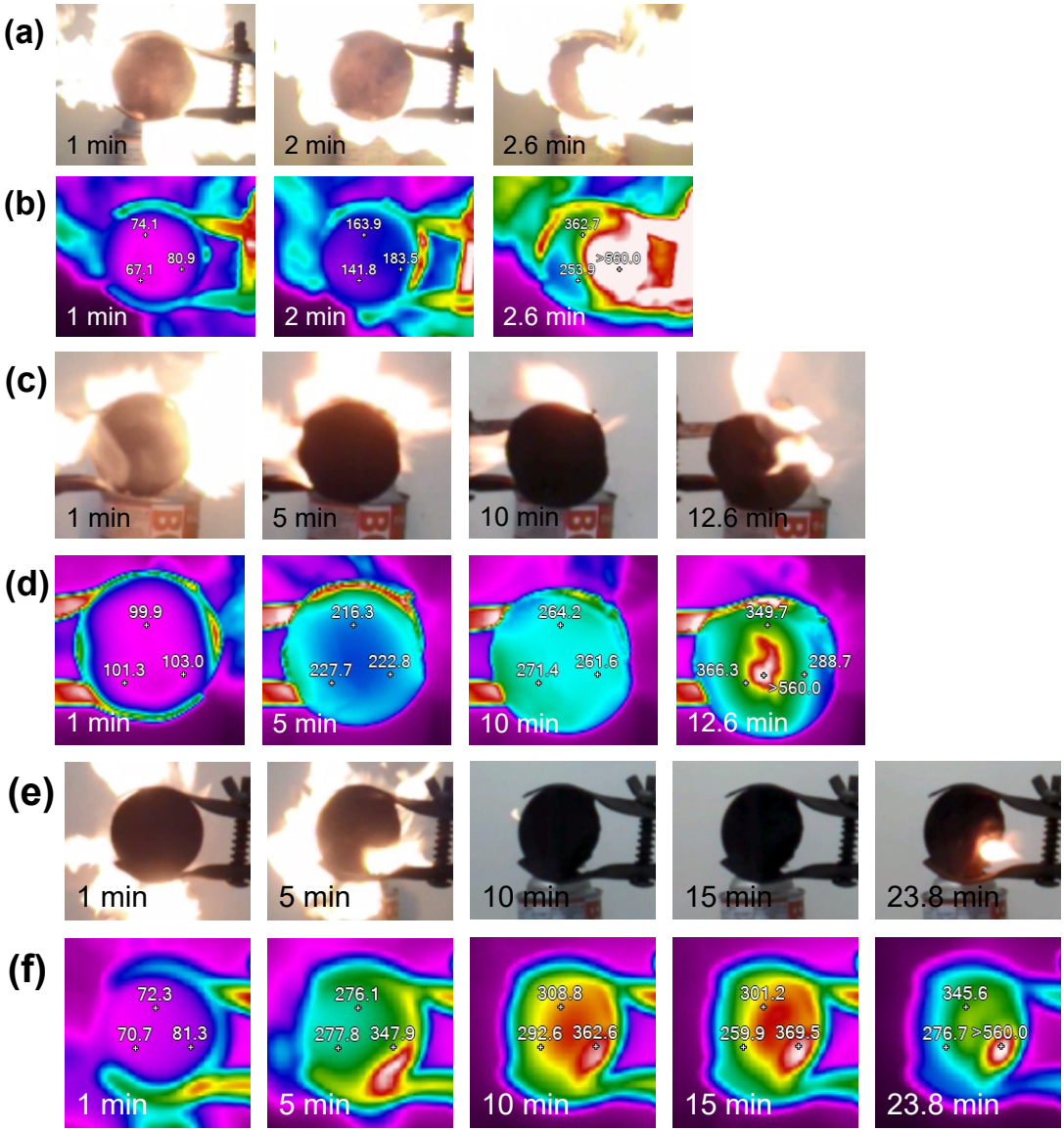

Figure S8. Photographs and the corresponding pseudo-color thermal images of the backside of (a, b) **EP**, (c, d) **EP/THA-Ni$_4$-3**, and (e, f) **EP/THA-Cu$_4$-3** sample at different times from 1min to the end of the butane torch test. The temperatures of the three points (T1, T2, and T3, in Celsius) in the pseudo-color images were used to represent the temperature change of the backside.

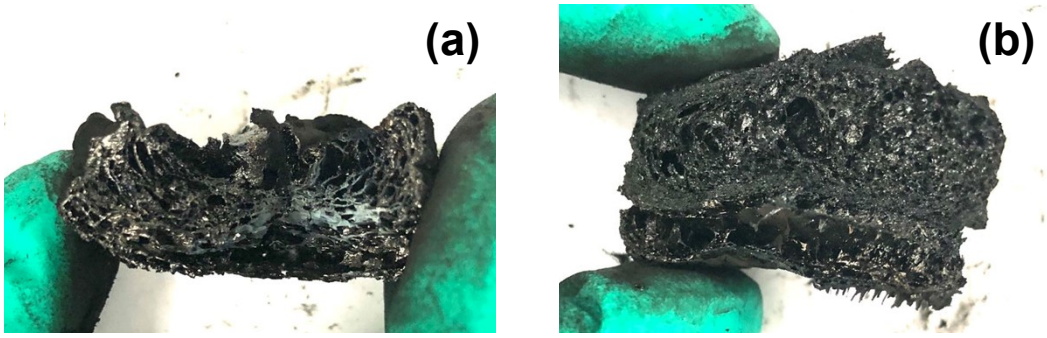

Figure S9. Cross-sections of (a) **EP/THA-Ni$_4$-3** and (b) **EP/THA-Cu$_4$-3** after the butane torch test.

The self-extinguishing and anti-dripping performance of the epoxy resin and its composites were evaluated by the UL-94 vertical burning test. A set of five specimens is required for the assessments. The neat epoxy could neither extinguish flame nor avert melt drips until the specimens were burned out, while the **EP/THA-Ni$_4$-3** and **EP/THA-Cu$_4$-3** composites undoubtedly demonstrated improved self-extinguishing performance and anti-dripping properties (Tables S4 and S5). More specifically, the combustion of **EP/THA-Ni$_4$-3** and **EP/THA-Cu$_4$-3** localized at the bottom corners of the specimens and the flame showed no tendency to grow larger or spread upward before it self-extinguished (see examples in Figures S10 and S11). After the tests, the specimens of **EP/THA-Ni$_4$-3** and **EP/THA-Cu$_4$-3** were barely burned except for being slightly charred at the ignited side (Figure S12).

Table S4. Detailed data of a set of five specimens of **EP/THA-Ni$_4$-3** from the UL-94 vertical burning test.

Specimen	Burning time after 1st ignition, t_1 (s)	Burning time after 2nd ignition, t_2 (s)	Dripping	Rating
1#	35	32	No	NR
2#	1	35	No	NR
3#	45	11	No	NR
4#	61	9	No	NR
5#	101	41	No	NR

Table S5. Detailed data of a set of five specimens of **EP/THA-Cu$_4$-3** from the UL-94 vertical burning test.

Specimen	Burning time after 1st ignition, t_1 (s)	Burning time after 2nd ignition, t_2 (s)	Dripping	Rating
1#	68	9	No	NR
2#	0	5	No	V0
3#	26	62	No	NR
4#	34	52	No	NR
5#	27	1	No	V1

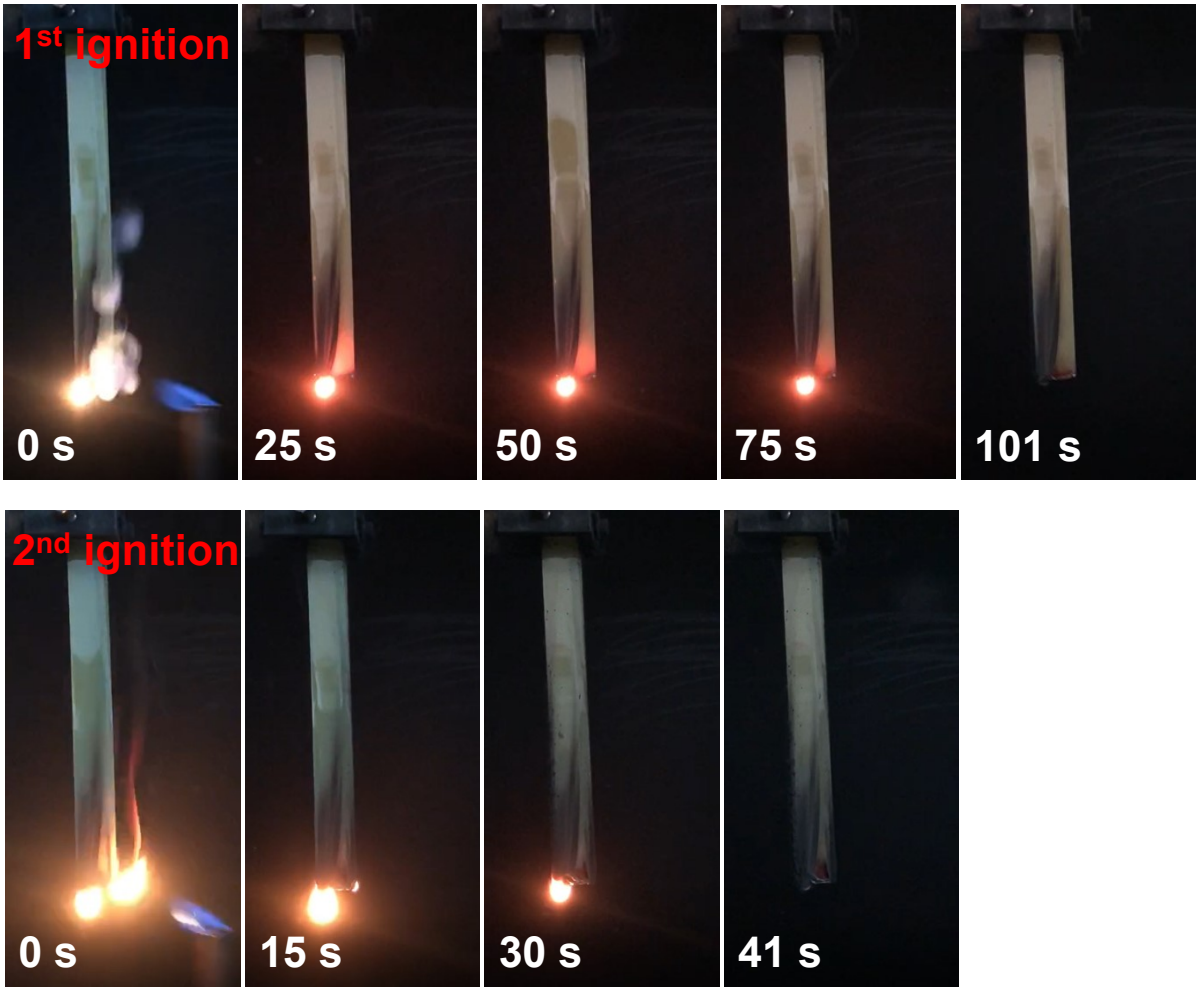

Figure S10. Combustion process of specimen 5# of **EP/THA-Ni$_4$-3** during the UL-94 vertical burning test. The sample displayed the longest burning time (t_1+t_2) among the five specimens.

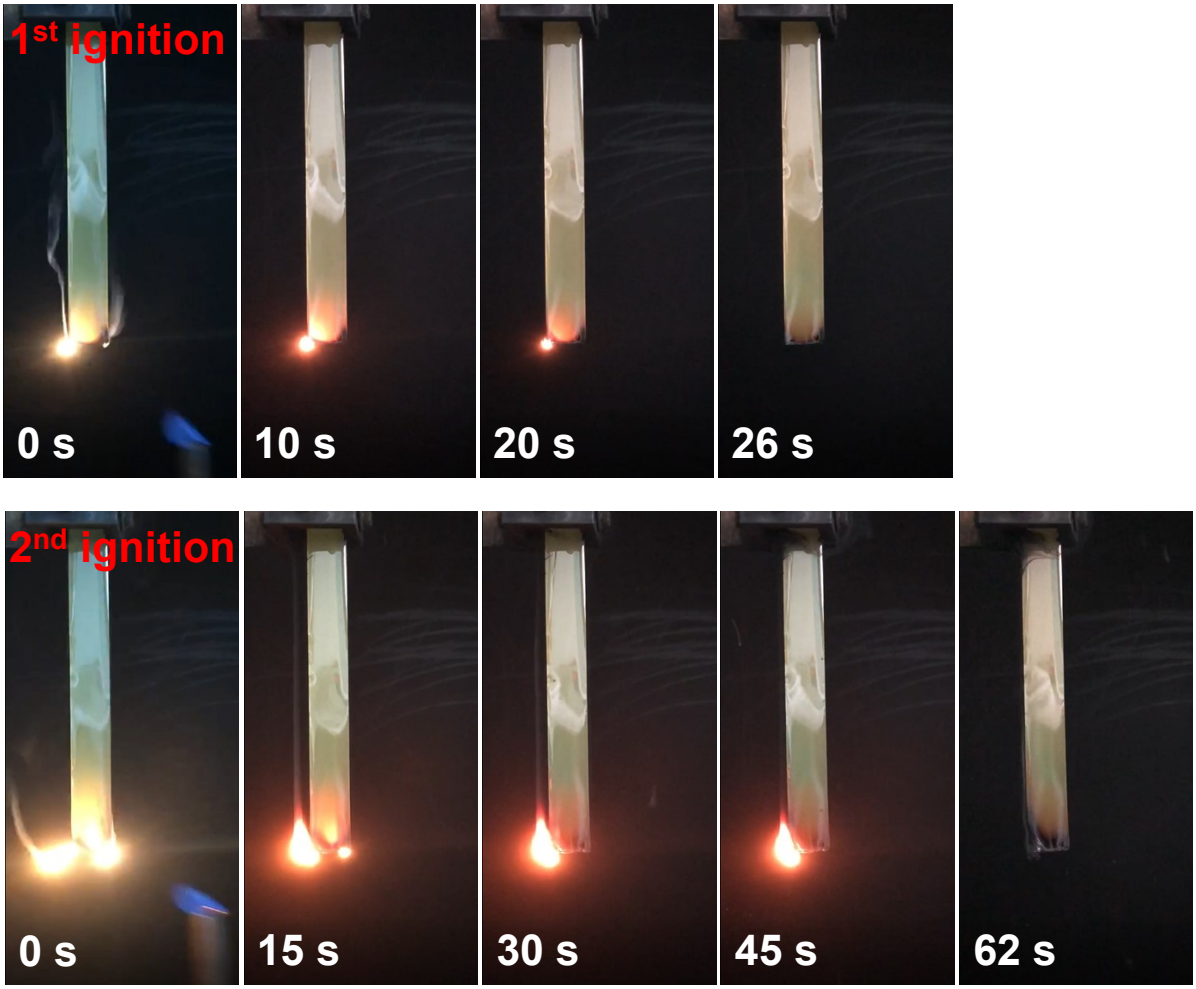

Figure S11. Combustion process of specimen 3# of **EP/THA-Cu$_4$-3** during the UL-94 vertical burning test. The sample displayed the longest burning time (t_1+t_2) among the five specimens.

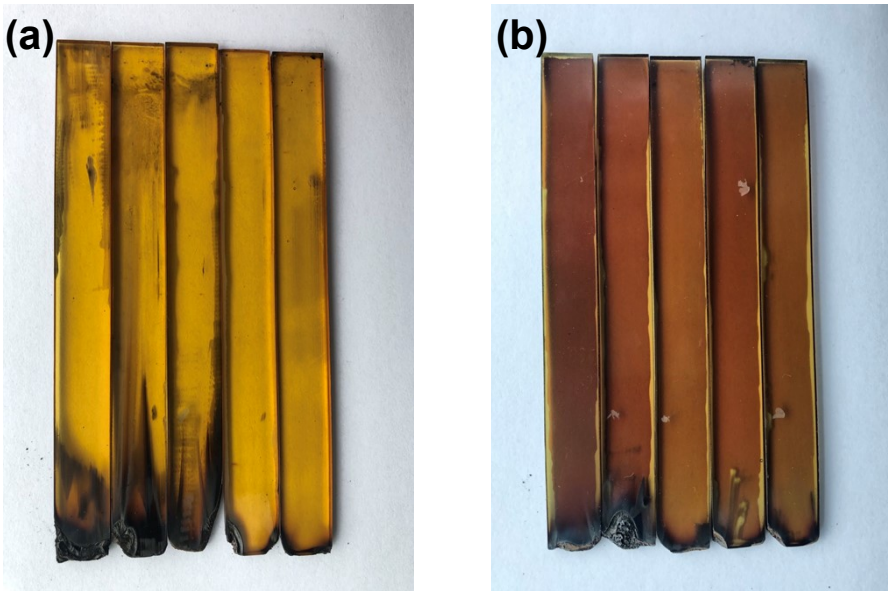

Figure S12. Photographic images of (a) **EP/THA-Ni$_4$-3** and (b) **EP/THA-Cu$_4$-3** specimens after the UL-94 vertical burning test.

The combustion behavior of the epoxy resin and its composites was investigated by cone calorimetry. Detailed data from the cone calorimetry and morphological structure of char residues are given below (Table S6, and Figures S13 and S14).

Table S6. Cone calorimetry of **EP**, **EP/THA-Ni$_4$-3**, and **EP/THA-Cu$_4$-3**.

Sample	TTI[a] (s)	*p*-HRR (kW/m^2)	t_p[b] (s)	AvHRR[c] (kW/m^2)	AvEHC[d] (MJ/kg)	THR (MJ/m^2)	TSP (m^2)
EP	49	964	135	223	22.5	90.2	38.6
EP/THA-Ni$_4$-3	49	714	95	169	26.7	68.6	23.6
EP/THA-Cu$_4$-3	49	753	110	183	20.8	74.6	30.6

[a] TTI is the time to ignition.

[b] t_p is the time to *p*-HRR.

[c] AvHRR is the average HRR between 49 to 450 s.

[d] AvEHC is the average effective heat combustion between 49 to 450 s.

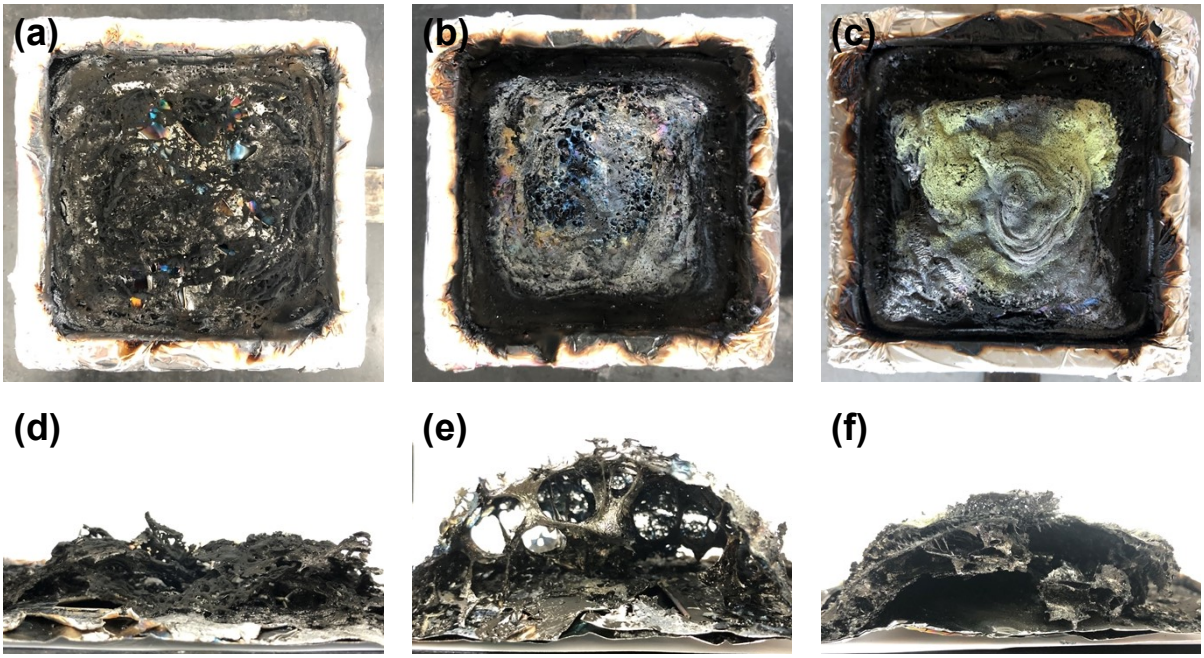

Figure S13. Char residues and their cross-sections of (a, d) **EP**, (b, e) **EP/THA-Ni$_4$-3**, and (c, f) **EP/THA-Cu$_4$-3** after the cone calorimetry.

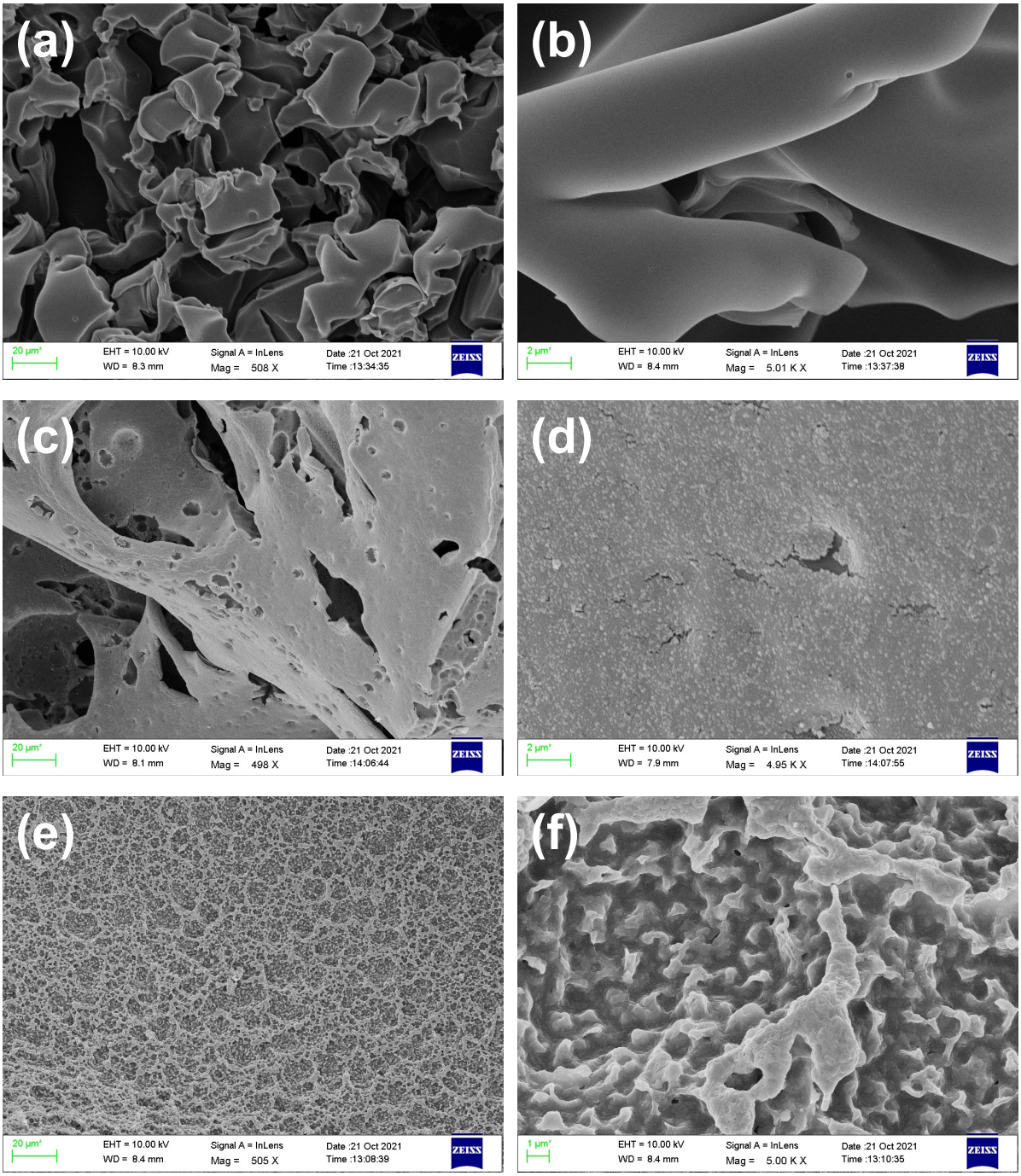

Figure S14. SEM images of char residues of (a, b) **EP**, (c, d) **EP/THA-Ni$_4$-3**, and (e, f) **EP/THA-Cu$_4$-3** after the cone calorimetry.

Table S7. Flame retardancy performance of the epoxy resin composites with different loading levels of **THA-Ni$_4$** and **THA-Cu$_4$**.

Sample	LOI (%)	UL-94		Cone calorimetry		
		t^a	Dripping	*p*-HRR (kW/m^2)	THR (MJ/m^2)	TSP (m^2)
EP	25.2	157	Yes	964	90.2	38.6
EP/THA-Ni$_4$-1	28.9	45	No	728	71.9	24.2
EP/THA-Ni$_4$-3	31.7	37	No	714	68.6	23.6
EP/THA-Ni$_4$-5	35.2	32	No	700	66.7	21.8
EP/THA-Ni$_4$-7	34.6	56	No	731	67.9	24.1
EP/THA-Cu$_4$-1	31.4	23	No	788	78.4	31.1
EP/THA-Cu$_4$-3	37.8	28	No	753	74.6	30.6
EP/THA-Cu$_4$-5	42.9	24	No	720	70.2	29.3
EP/THA-Cu$_4$-7	39.6	42	No	734	73.8	28.2

[a] Average burning time after ignition of the five specimens.

3.4. Chemical states of char residues

The chemical states of the char residues after the cone calorimetry were studied by X-ray photoelectron spectroscopy (Figure S15).

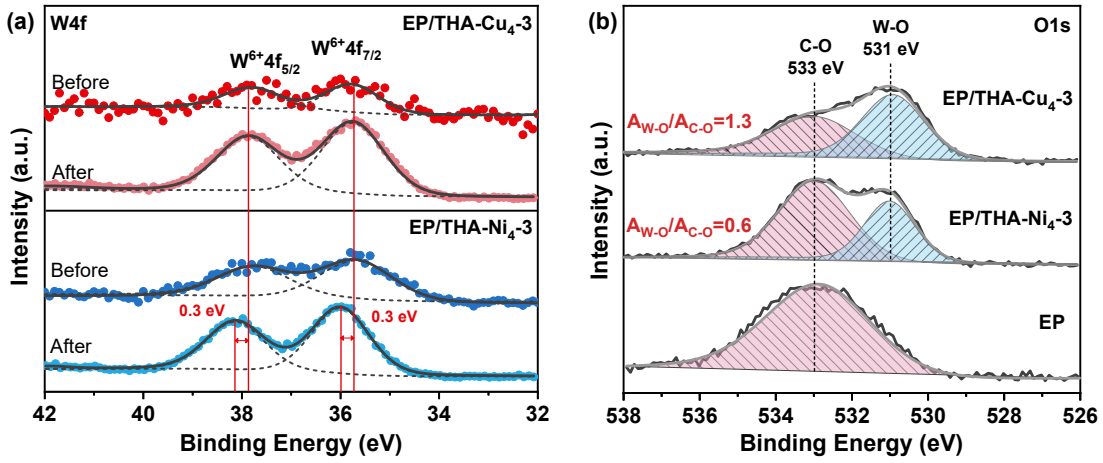

Figure S15. XPS spectra of (a) W 4f and (b) O 1s of the char residues from the cone calorimetry of **EP**, **EP/THA-Ni$_4$-3**, and **EP/THA-Cu$_4$-3**.

3.5. Pyrolysis products

The gaseous products evolved from the pyrolysis of **EP**, **EP/THA-Ni$_4$-3**, and **EP/THA-Cu$_4$-3** were investigated by thermogravimetric analysis-infrared spectrometry (TG-FTIR). Figure S17 shows the absorbance of their main products during the time.

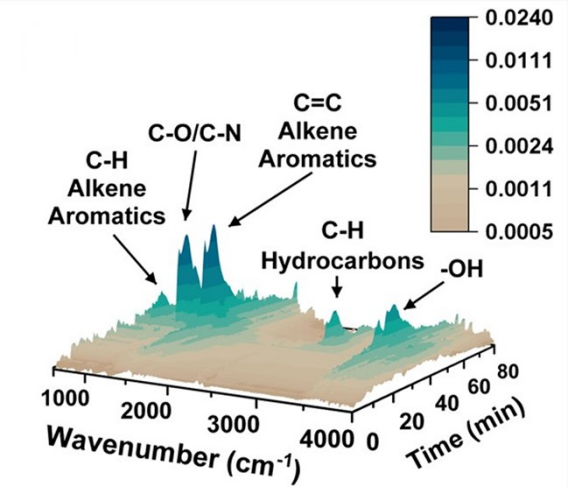

Figure S16. Three-dimensional TG-FTIR spectra of **EP/THA-Ni$_4$-3**.

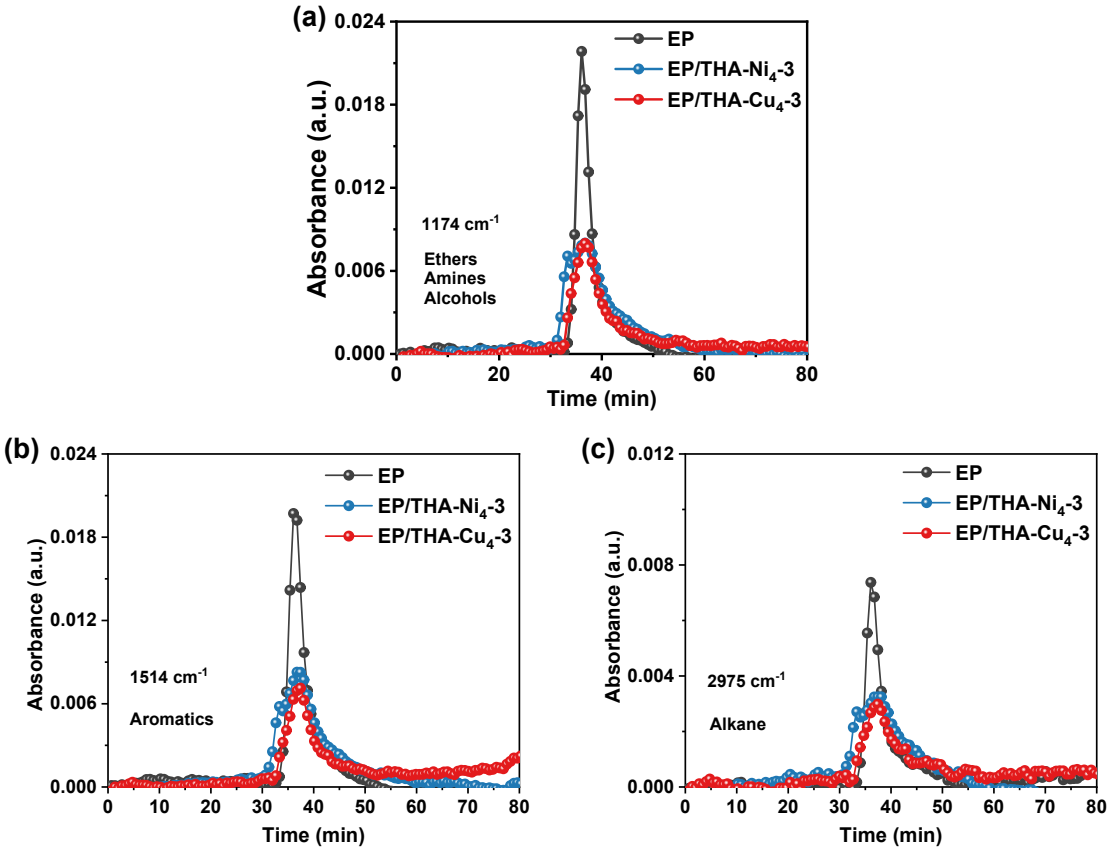

Figure S17. Absorbance intensities of main gaseous products of **EP**, **EP/THA-Ni$_4$-3**, and **EP/THA-Cu$_4$-3** as a function of time.

3.6. Comparison with various flame retardants

The flame retardancy performance of **THA-Ni$_4$** and **THA-Cu$_4$** were compared with redox-inactive POM-ILs (**THA-P$_2$W$_{18}$** and **THA-Zn$_4$**) and the commercial flame retardants (aluminum hydroxide (ATH), triphenyl phosphate (TPP), and decabromodiphenyl ethane (DBDPE)) (Table S8). The ATH, TPP, and DBDPE were selected as the representatives of inorganic, organic phosphorus, and halogen-based flame retardants, respectively.

Table S8. Flame retardancy performance of epoxy resin retarded with redox-inactive POM-ILs and commercial flame retardants.

Sample	t (min)[a]	LOI (%)	UL-94		Cone calorimetry		
			t (s)	Dripping	*p*-HRR (kW/m^2)	THR (MJ/m^2)	TSP (m^2)
EP	~2	25.2	157	Yes	964	90.2	38.6
EP/TPP-3	~5	33.0	68	No	975	79.2	38.9
EP/ATH-3	~3	27.3	145	Yes	865	83.9	37.5
EP/DBDPE-3	~5	29.9	8	No	957	78.5	35.5
EP/THA-P$_2$W$_{18}$-3	~3	27.8	125	Yes	976	76.6	39.0
EP/THA-Zn$_4$-3	~6	31.0	89	No	867	80.4	30.8
EP/THA-Ni$_4$-3	**~12**	**31.7**	**37**	**No**	**714**	**68.6**	**23.6**
EP/THA-Cu$_4$-3	**~24**	**37.8**	**28**	**No**	**753**	**74.6**	**30.6**

[a] Burning time before flame breakthrough in the fire-resistance experiments.

3.7. Migration resistance

The migration resistance of **EP/THA-Ni$_4$-3** and **EP/THA-Cu$_4$-3** composites were assessed with accelerated aging tests (Table S9 and Figure S18).

Table S9. Mass loss and LOI values of **EP/THA-Ni$_4$-3** and **EP/THA-Cu$_4$-3** after the accelerated aging tests.

Aging time	EP/THA-Cu$_4$-3		EP/THA-Ni$_4$-3	
	Mass loss (%)[a]	LOI (%)	Mass loss (%)	LOI (%)
0 h	0	37.8±0.2	0	31.7±0.3
24 h	0.037±0.015	37.2±0.2	0.030±0.007	31.8±0.2
72 h	0.051±0.013	37.5±0.3	0.026±0.014	31.5±0.2
168 h	0.062±0.009	36.9±0.3	0.021±0.013	31.3±0.3

[a] defined as the ratio (in percentage) of the mass loss to the original mass.

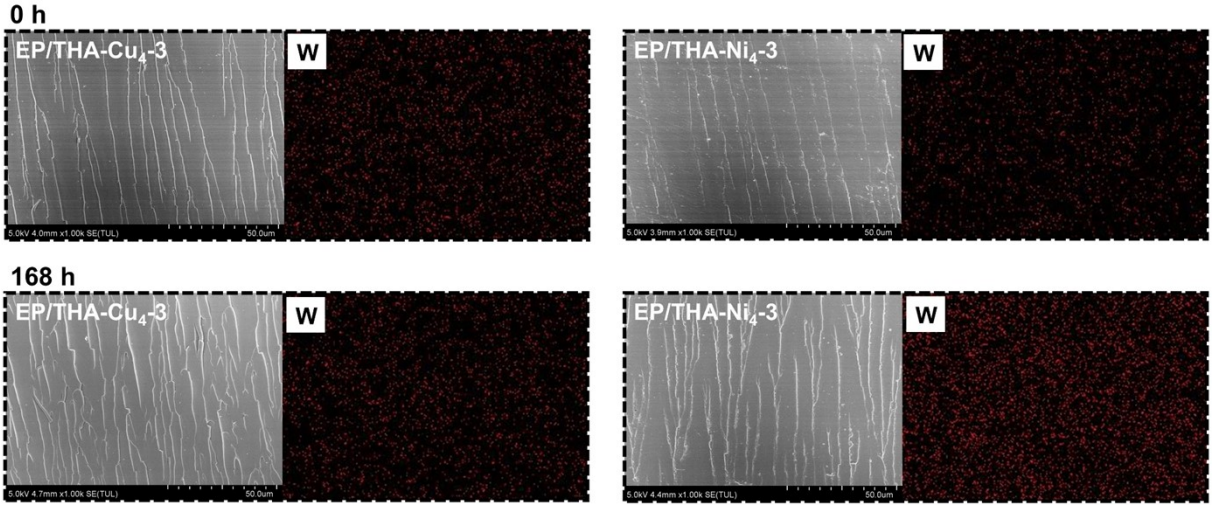

Figure S18. SEM and element mapping images of **EP/THA-Ni$_4$-3** and **EP/THA-Cu$_4$-3** before and after 168 h aging tests.

4. Reference

[1] R. G. Finke, M. W. Droege, P. J. Domaille, *Inorg. Chem.* **1987**, *26*, 3886–3896.

[2] H. Lv, Y. Gao, W. Guo, S. M. Lauinger, Y. Chi, J. Bacsa, K. P. Sullivan, M. Wieliczko, D. G. Musaev, C. L. Hill, *Inorg. Chem.* **2016**, *55*, 6750–6758.

[3] H. Lv, W. Guo, K. Wu, Z. Chen, J. Bacsa, D. G. Musaev, Y. V. Geletii, S. M. Lauinger, T. Lian, C. L. Hill, *J. Am. Chem. Soc.* **2014**, *136*, 14015–14018.

[4] D. E. Katsoulis, M. T. Pope, *J. Am. Chem. Soc.* **1984**, *106*, 2737–2738.